Assessment of ground deformation and seismicity associated to fluid injection and oil/gas extraction in the Argentinian Patagonia

Guillermo Tamburini-Beliveau (guillermotb@conicet.gov.ar)
Centro de Investigaciones y Transferencia de Santa Cruz (CIT SC - CONICET)
Javier A. Grosso-Heredia
Universidad del Comahue
Marta Béjar-Pizarro
Geological Survey of Spain
Raúl Pérez-López
Geological Survey of Spain
Juan Portela-Fernández
Universidad Politécnica de Madrid, Natural Hazards and Risks
Martín Cismondi-Duarte
Instituto de Investigación y Desarrollo en Ingeniería de Procesos y Química Aplicada (IPQA-CONICET-UNC). Ciudad Universitaria
Oriol Monserrat
Centre Tecnològic de Telecomunicacions de Catalunya

Article

Keywords:

Posted Date: March 15th, 2022

DOI: https://doi.org/10.21203/rs.3.rs-1435139/v1

Title

Assessment of ground deformation and seismicity associated to fluid injection and oil/gas extraction in the Argentinian Patagonia

Guillermo Tamburini-Beliveau[*] , mail: guillermotb@conicet.gov.ar
Centro de Investigaciones y Transferencia de Santa Cruz (CIT SC - CONICET), Lisandro de la Torre 860, Río Gallegos, Argentina.

Javier A. Grosso-Heredia, mail: javieragrosso@gmail.com
Universidad del Comahue, Departamento de Geografía, Buenos Aires 1400, Neuquén, Argentina.

Marta Béjar-Pizarro, mail: m.bejar@igme.es
InSARlab Geohazards InSAR laboratory Geohazards group Geoscience Research dept., Geological Survey of Spain C/Alenza 1 28003 Spain

Raúl Pérez-López, mail: r.perez@igme.es
InSARlab Geohazards InSAR laboratory Geohazards group Geoscience Research dept., Geological Survey of Spain C/Alenza 1 28003 Spain

Juan Portela-Fernández, mail: jj.portela@upm.es
Universidad Politécnica de Madrid, RG Terra: Geomatics, Natural Hazards and Risks, Mercator 2, 28031 Madrid, Spain.

Martín Cismondi-Duarte, mail: martin.cismondi@unc.edu.ar
Instituto de Investigación y Desarrollo en Ingeniería de Procesos y Química Aplicada (IPQA-CONICET-UNC). Ciudad Universitaria. Córdoba, Argentina.

Oriol Monserrat: mail: omonserrat@cttc.cat
Centre Tecnològic de Telecomunicacions de Catalunya, Departament de Geomàtica, Carl Friedrich Gauss 7, Castelldefels, Spain.

Abstract

The exploitation of both conventional and non-conventional hydrocarbons may lead to still not well-known environmental consequences such as ground deformation and induced/triggered seismicity. Identifying and characterizing these effects is fundamental for prevention or mitigation purposes, especially when they impact populated areas. Two case studies of such effects on hydrocarbon-producing basins in Argentina, the Neuquén and the Golfo de San Jorge, are presented in this work. The intense hydrocarbon production activities in recent years and their potential link with the occurrence of two earthquakes of magnitude 4.9 and 5 near the operating well fields is assessed. A joint analysis of satellite radar interferometry and records of fluid injection and extraction demonstrate that, between 2018 and 2020, vertical ground displacements occurred in both study areas over active well fields that might indicate a correlation to hydrocarbon production activities. Coseismic deformation models of the two earthquakes constrain source depths to less than 2 km. The absence of seismicity before the beginning of the hydrocarbon activities in both areas, and the occurrence of the two largest and shallow earthquakes in the vicinity of the active well fields just after intensive production periods, points towards the potential association between both phenomena.

Introduction

Hydrocarbons are a highly demanded raw material and the exploitation of basement reservoirs for hydrocarbon production is a fundamental industrial activity. However, the

economic and social benefits of its extraction are often accompanied by undesirable consequences such as environmental impacts and social unrest. The anticipation to these collateral effects is key to ensure the good performance of the hydrocarbon production activities.

The literature illustrates various examples of geohazards triggered by the hydrocarbon industry around the globe such as ground displacements associated with fluid injection and extraction (Kim et al. 2018, Shirzaei et al. 2016, Semple et al. 2017); and seismicity correlated to the injection of wastewater and enhanced oil recovery (Weingarten et al. 2015), to shale gas hydraulic fracturing (Lei et al. 2017, Atkinson et al. 2016, Mulargia & Bizzarrini 2014), and to hydraulic stimulation for enhanced geothermal systems, which operates in a similar way to hydrocarbon production (Samsonov et al. 2017, Grigoli et al. 2018). Maximum magnitudes of earthquakes triggered by these activities can reach significant rates, as occurred in Oklahoma in November 2011, with a Mw 5.7 earthquake related to wastewater injection (Keranen et al.2013) or in Mexico in 2011, with a Mw 7.2 earthquake related to fluid extraction at a geothermal field (Samsonov et al. 2017).

Three of the five hydrocarbon-producing basins of Argentina are located in Patagonia. The Neuquén basin in North Patagonia was one of the first exploitations in Argentina. The operations started at the very beginning of the 20th century continuing up to date. The non-conventional exploitation of tight and shale geological formations in the basin started in 2011. The estimated non-conventional reserves of the Neuquén basin are 9000 billion of natural gas m^3 and 2.5 billion of m^3 oil. According to the US Energy Administration, these formations are the second biggest of shale gas and the fourth of shale oil at global scale (YPF 2021). The initiation of the hydraulic fracturing in the Vaca Muerta formation, a well-known shale formation in the Neuquén basin, has been followed by a significant increase of the seismic activity, see Figure 1 A.

In South Patagonia, the Golfo de San Jorge (GSJ) basin is also a historical hydrocarbon-producing basin, where more than forty thousand wells have been drilled since the first perforations started searching for water in this arid region. Unlike the Neuquén basin, only conventional resources are exploited here (Figure 1B).

Despite the intensive hydrocarbon activity carried out in these basins, a lack of comprehensive analysis on the risk of triggering geohazards such as ground deformation and induced seismicity is obvious. Only two publications addressed the topic in the Neuquén basin (Correa-Otto 2021 and Vázquez et al. 2020) and none in the GSJ basin. The recent occurrence of two significant earthquakes within the hydrocarbon production fields in these two basins, the M_L 5 2019 October 17 earthquake, near the town of Las Heras in the GSJ basin, and the M_L 4.9 2019 March 7 event, near the village of Sauzal Bonito in the Neuquén basin (Figure 1), have caused social unrest among the population. It is worth noting that these areas are located in the extra-Andean low seismic region, and that no previous earthquakes had been reported prior to the beginning of the hydrocarbon production activities.

This study aims to analyse the relationship between hydrocarbon activities and its effects on the surface: ground displacements and the irruption of new seismic processes

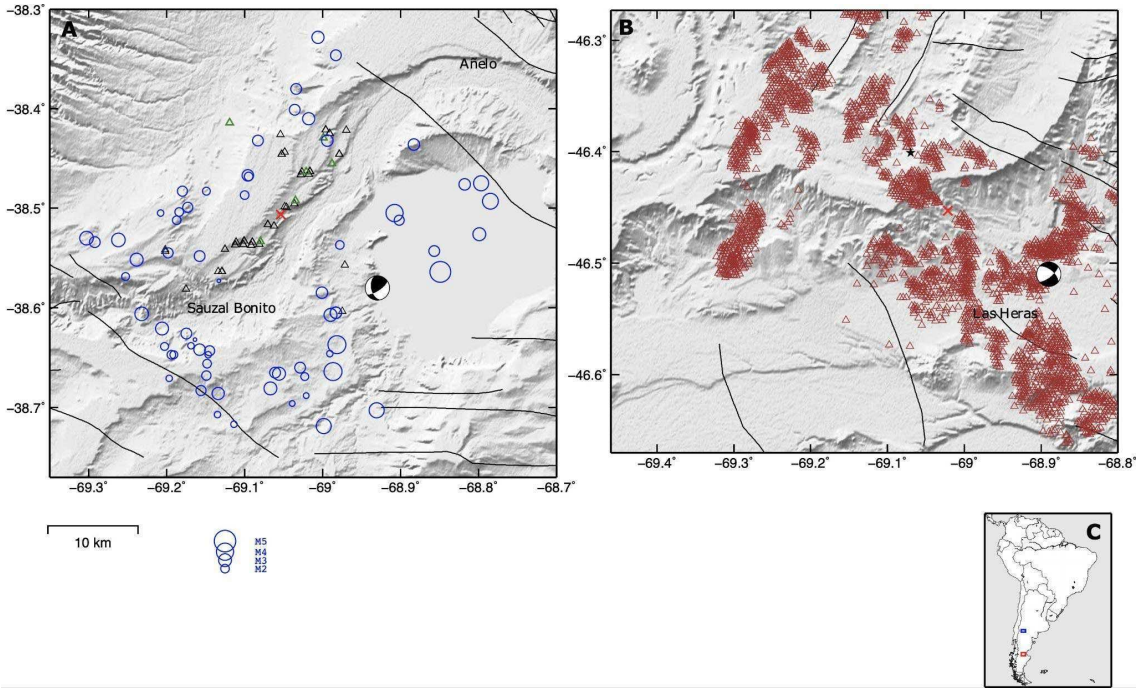

Figure 1. Study areas in the Argentinian Patagonia. Data are plotted on SRTM topography (Farr and Kobrick 2000) displayed in shaded relief. (A) Neuquén basin area. Blue circles represent epicenters of seismic events scaled by local magnitude (M_L) occurred in the period November 2015 to November 2020, from the Instituto Nacional de Prevención Sísmica (INPRES) catalog. The red cross indicates the reference point for the 15-km screening criterion analyzed in figure 3. The location of fracking (black triangles) and wastewater (green triangles) wells is also shown (Secretaría de Energía). Black lines indicate the main tectonic faults from Silvestro and Zubiri (2008). The Global Centroid Moment Tensor (GCMT) focal mechanism of the 07/03/2019 earthquake (M_L 4.9, M_w 5) is shown. (B) Golfo de San Jorge area. Brown triangles represent production wells. Black lines indicate the main tectonic faults (Allard et al, 2020). The red cross indicates the reference point for the 5-km distance limit analyzed in figure 3. The Global Centroid Moment Tensor (GCMT) focal mechanism of the 17/10/2019 earthquake (M_L 5, M_w 4.9) is shown. (C) Inset map showing the region of South America with the two study areas delineated in blue (Neuquén basin) and red (GSJ basin).

in the two basins. For this purpose, records of fluid injection and extraction, number of hydraulic fractures, seismicity and ground movements measured with Satellite Synthetic

Aperture Radar Interferometry (DInSAR) data are jointly analised. Different periods of observation have been evaluated depending on the specific characteristics of each of the case studies and the data available, expanding from 2015 to 2021.

This article is organised with the following structure. The results of our analysis are presented in the next section with a subsection dedicated for each case study, starting with the Neuquén basin and followed by the GSJ basin. Each sub-subsection is firstly dedicated to the analysis of ground displacements, and secondly to seismicity, both linked to hydrocarbon production trends. Finally, the results are discussed, and the conclusions are presented.

Results

The Neuquén basin

The available dataset analysed in the Neuquén basin include displacement measurements obtained with Differential Synthetic Aperture radar interferometry (DInSAR), Persistent Scatterer interferometry (PSI), seismic data and monthly volume production of conventional and non-conventional wells. We focused the analysis on a region surrounding the epicenter of the main earthquake (7th of March of 2019), which has experienced a sudden and extraordinary increase of hydrocarbon production, a high concentration of seismic events and where two areas affected by ground displacements have been observed.

Figure 2 shows the displacement velocity maps obtained through a PSI analysis, performed with the PSIG software (Devanthéry et al. 2014), exploiting the ascending and descending trajectories of Sentinel-1 data. The color scale represents the velocities of displacement of each point in mm/year. Displacements are shown in the satellite's Line-Of-Sight (LOS), which means that the measurements represent the projection of the real displacements along the satellite-point line.

The results presented in Figure 2 allowed the identification of two ellipsoidal shape ground displacement phenomena, with an approximate radius of 2.3 km, that were active during the entire analysed period. In these areas, identified by the numbers 1 and 2 in Figure 2, a high number of new fracking wells have been drilled. The analysis of these deformation phenomena is provided in section "*Hydrocarbon production in the Neuquén basin and surface deformation*". The PSI analysis allowed the identification of a third feature, labelled number 3 in Figure 2, which is related to coseismic deformation caused by the 2019 March 7 earthquake, which is discussed later in this document. Figure 2 (a and b) shows the ground displacement velocity map obtained by exploiting Sentinel-1 imagery acquired in ascending, i.e., satellite travelling from south to north in right looking mode, and descending trajectory, i.e., satellite travelling from north to the south in right looking mode, respectively. The results refer to the periods February 2018 to April 2020 in the ascending dataset and October 2018 to April 2020 in the descending one. The precision of the estimated velocities is about ±1.3 mm/year in the ascending trajectory and ±2.2 mm/year in the descending one.

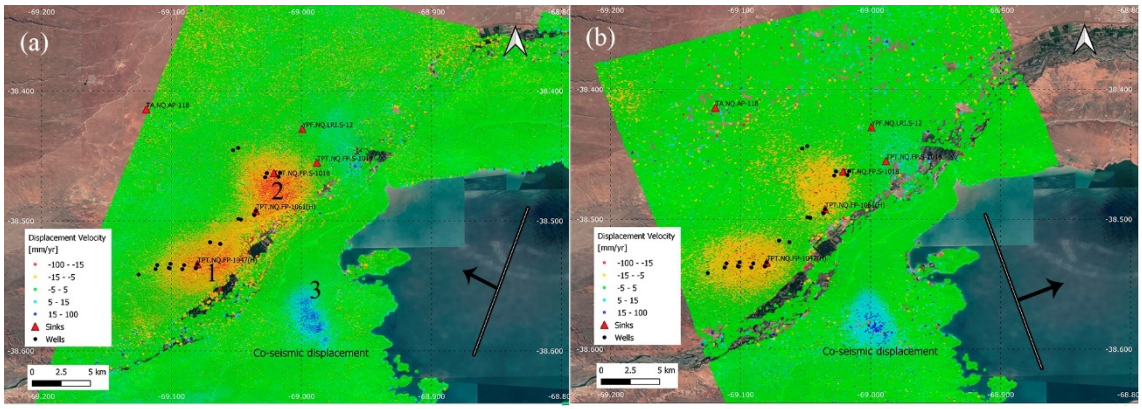

Figure 2. Average Line-Of-Sight (LOS) ground displacement velocity maps obtained exploiting the PSI techniques observed with a descending trajectory spanning the period from February 2018 to April 2020 (a) and with an ascending trajectory from October 2018 to April 2020 (b). Positive and negative LOS values represent ground displacements towards and away from the satellite, respectively. Main deformation zones labelled 1 and 2 correspond to areas with high concentration of wells, 33 and 25 respectively (see Figure 1). Label 3 indicates the main area affected by the M_L 4.9, 2019 March 7 earthquake.

Figure 3 (a) shows the harmonised hydrocarbon production data in the Neuquén basin study area during the period 2015-2020: monthly extraction (conventional and non-conventional), SWD injection and fracking injection. The harmonisation procedure is described in the Methods section. The main seismic events have also been depicted as vertical lines. Figure 3 (b and c) displays the time series of ground deformation obtained from the ascending and descending trajectories in zones 1 and 2, respectively, together with the curve of the total accumulated gas extraction for each area. The latter parameter has been standardised (normalised and scaled) to better show the parallelism between both processes. The normalisation is described in the Methods section.

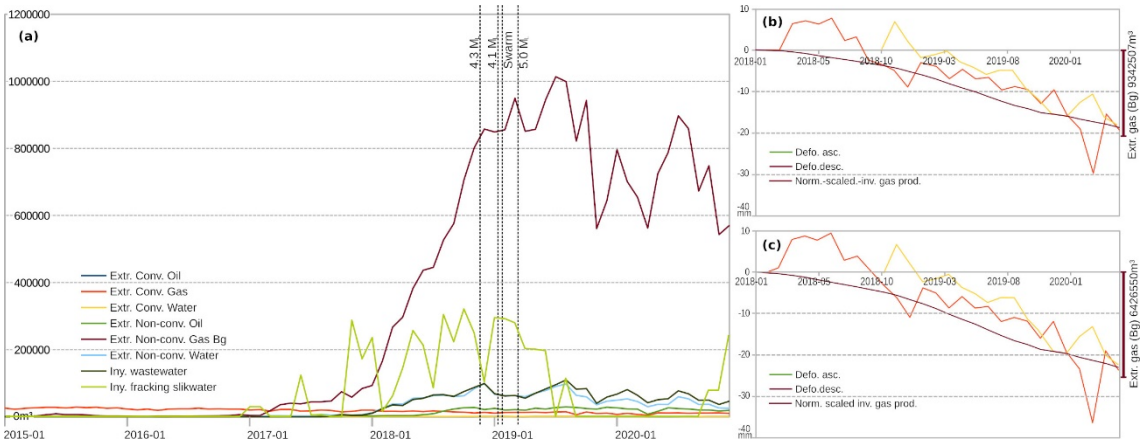

Figure 3. (a) Temporal evolution of hydrocarbon production (in m^3) during the period 2015 – 2020 in the Neuquén basin. Main seismic events in the area are shown as vertical dashed black lines. Panels (b) and (c) show the time series of ground deformation for zones 1 and 2, respectively, during the period 2018-2020 together with monthly accumulated non-conventional gas production. This last curve has been normalised, from 0 to 1 for the time span, and inversely scaled to fit the same nominal scale as deformation patterns. The vertical scale bar in the right axis of figures (b) and (c) provide information on the total accumulated volumetric amount (m^3) of non-conventional gas extracted.

Hydrocarbon production and ground displacements in the Neuquén basin

The trends of deformation of zones 1 and 2 revealed to be affected by ground displacements in Figure 2 can be observed in the time series displayed in Figure 3 (b) and (c), respectively. These time series show that the temporal behaviour is almost linear during the entire analysed period. For these time series, the estimated precision is 6.3 mm and 3.6 mm for descending and ascending trajectories respectively. The lower precision of the descending dataset is explained by a lower number of images and a shorter period of observations. The average accumulated displacement for zone 1 during the period October 2018 to April 2020 is 19.0 mm and 17.8 mm in ascending and descending trajectories, respectively. The average velocity in zone 1 is -10.5 mm/yr in the ascending trajectory and -12.8 mm/yr in the descending one with maximum velocities of deformation reaching up to 40 mm/yr in LOS in the centre of the ellipsoidal areas. The differences in velocity between both trajectories are related to the estimated precision. Similar figures are obtained for zone 2. The comparison between both trajectories confirms the reliability of the results and confirms that the displacements in zones 1 and 2 are almost vertical and therefore can be interpreted as subsidence.

Figure 3 (a) shows the beginning of non-conventional activity in January 2017. A clear change in the trend occurred in July 2017 with the initiation of strong fracking visible in the first high injection peak and reflected in the later increase in the gas extraction

(around the beginning of 2018). Zones 1 and 2 are affected by the accumulated action of multiple wells working simultaneously but in different stages of the production chain (fracturing or extracting). Considering the period framed in Figure 3 (a), the predominant activity in terms of subsurface volume changes is gas extraction. Therefore, the expected surface displacements triggered in this period is subsidence (Samsonov et al. 2017; Baranova et al. 2011), which is observed in zones 1 and 2 in Figure 2, and in the displacements trends displayed in Figure 3 (b and c).

To confirm the relationship between ground displacements and gas extraction, we analyzed the DInSAR results over zones 1 and 2 before the operations started. The period October 2016 to March 2018 was processed using the Parallel Small BAseline Subset (P-SBAS) on-demand processing chain (Casu et al. 2014, Manunta et al. 2019) as presented in the Methods annex. The results are shown in Figure S1 of the supporting material. The measured displacements in the area were negligible, displaying average velocities of 1 mm/year with a standard deviation 3 mm/yr in zone 1 and 2. The ground stability observed in this period coincides with an insignificant activity of the wells. Therefore, there is sufficient evidence to conclude that there is a relationship between ground surface displacements and hydrocarbon production activities.

Hydrocarbon production in the Neuquén basin and the associated seismic events

The analysis of multiple source seismic catalogues (INPRES 2021a, USGS 2021, ISC 2021) reveals that no earthquakes were registered in the study area before 2015. This quiescence suddenly changed with the intensification of hydraulic fracturing activities in the area (Correa-Otto, 2021; Vásquez et al. 2020), as shown in Figure 1. Therefore, we investigate the relationship between the hydrocarbon activities and the observed seismicity.

Seismic sequences potentially classified as induced seismicity normally show a temporal and spatial relationship with the underground injection and industrial operations (Ellsworth 2013, Atkinson et al. 2015, Weingarten et al. 2015). To investigate the potential relationship between seismicity and hydrocarbon activities in the study area, the seismic events recorded by the National Institute of Seismic Prevention of Argentina (Instituto Nacional de Prevención Sísmica, INPRES) during the period November 2015 to November 2020 are analyzed. A total of 63 earthquakes were registered in this period, with a maximum earthquake of local magnitude (M_L) 4.9 (at 7 km depth), and a magnitude of completeness (Mc) 2.4. The earthquake depth ranges from 1.1 to 22 km, with an average of 6 km. The average depth for fluid and sands injection in the hydraulic fracturing procedure is about 3 km, with a horizontal subsurface branch of the wells of 2 km in average. The analyses of earthquake statistical basic parameters (the b-value of the Gutenberg-Richter law, the maximum earthquake, magnitude of completeness, earthquake's depth distribution and hydraulic depth operations and horizontal longitude) are included in the Figure S3 of the supplementary information of this article. The b-value obtained is 0.66 (correlation coefficient of 0.94). However, the number of earthquakes is not enough to determine the significance of this value in relation to other bibliographic values (Mousavi et al., 2017).

The temporal relationship between fracking underground operations and earthquake occurrence, for the period January 2015 to December 2020, is shown in Figure 4. The

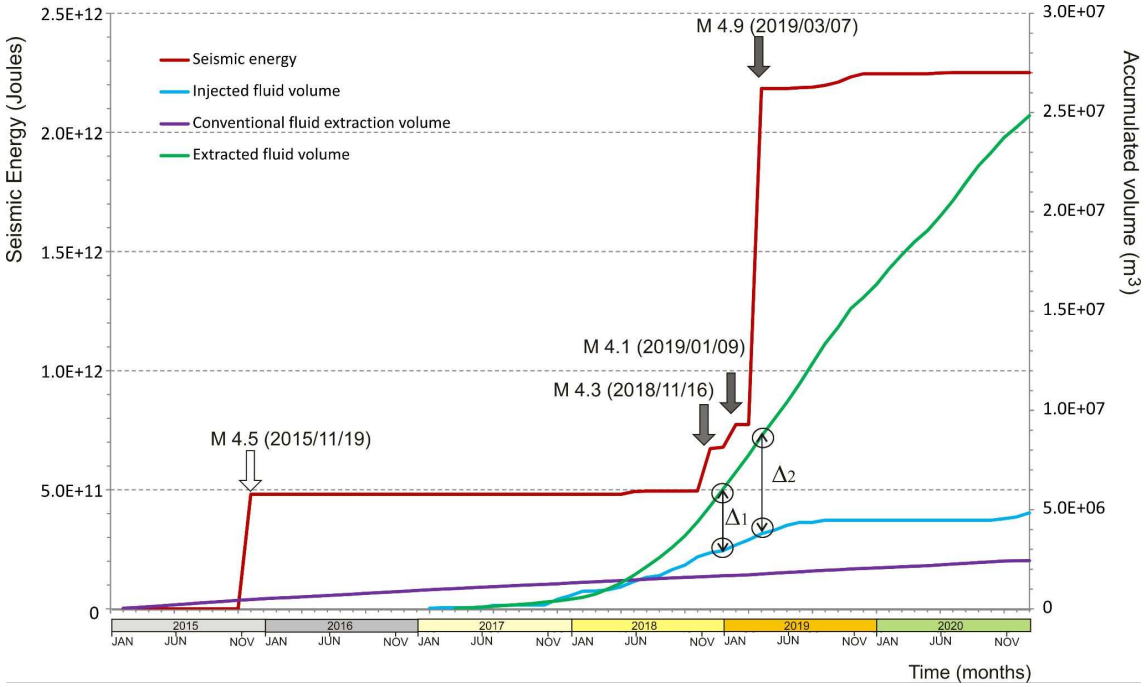

Figure 4. Accumulated seismic energy released (in Joules) recorded by INPRES between 2015 and 2020, versus different underground operations within the Neuquén basin study area (in m^3). Blue and green lines show injected and extracted fluid volume, respectively, using non-conventional methods. Purple line shows extracted fluid volume using conventional methods. The production data used for this figure are the same used in Figure 3.

accumulated seismic energy is compared with accumulated volumes of injection/extraction of fluids during both conventional and non-conventional hydrocarbon production activities.

The 2019 earthquakes (M_L 4.1 and M_L 4.9) coincide with a sharp increase of the extracted volume, which could be related to the earthquake triggering, in addition to the increase of the balance between injected/extracted volume. Also, and related to the decrease of fracking injection, the seismic energy decreased to a low threshold without relevant earthquakes of M_L > 3.6. The proximity in time between the M_L 4.1 (2019/01/09) and the M_L 4.9 (2019/03/07) earthquakes, could suggest a triggering of an anticipated earthquake (the last one) by the previous one (induced earthquake). This could explain the high seismic energy released in the M_L 4.9 earthquake. Nevertheless, it is not possible to discriminate between induced or anticipated earthquakes from this analysis (Fig. 4).

The largest seismic event registered in the study area occurred on 7 March 2019 at 05:10:37 UTC, with local magnitude M_L4.9, according to INPRES and moment magnitude M_w of 5 according to the USGS (USGS, 2021). The location of the epicenter and depth of the earthquake varies among different agencies (USGS: latitude 38.523°S, longitude 68.857°W, 13.8 km depth; INPRES: latitude 38.563°S, longitude 68.833°W, 7 km depth; Vásquez et al. 2020: latitude 38.529°S, longitude 68.891°W, 10.3 km depth).

This seismic event produced ground deformation measurable with InSAR data. We used the coseismic interferograms to constrain the earthquake source parameters. Figure 5 shows ground deformation associated with the earthquake in both ascending and

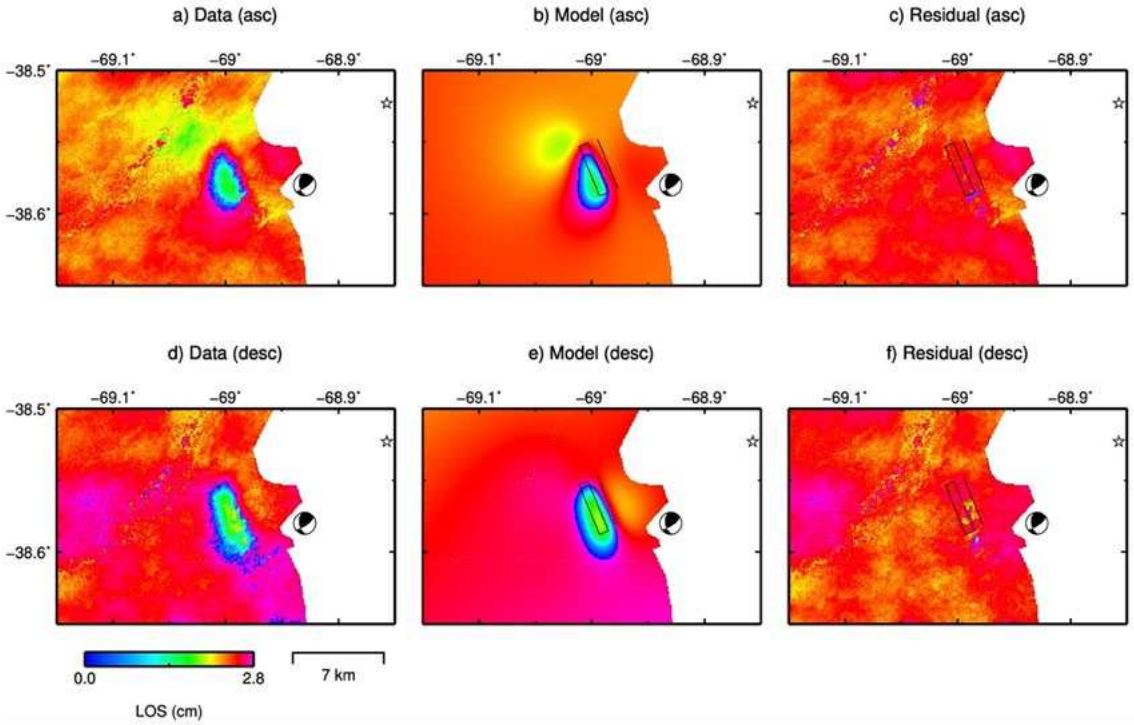

Figure 5. (a) and (d) show coseismic Line-Of-Sight (LOS) deformation of the Mw 5, 2019 March 7 Neuquén basin earthquake obtained as the average of 11 coseismic ascending interferograms (in a) and as the average of 10 coseismic descending interferograms (in d). (b) and (e) show LOS deformation predicted by the forward model using the maximum a posteriori probability solution. (c) and (f) show the residuals. The black rectangle represents the outline of the optimal fault plane. The Global Centroid Moment Tensor (GCMT) is represented by the beach ball.

descending geometry. This deformation pattern corresponds to a main lobe with a maximum ground displacement of ~ 22 mm towards the satellite.

This deformation pattern can be explained using a uniform slip rectangular dislocation centered at latitude 38.5691°S, longitude 68.9982°W (Fig. 5) and at 1.2 km depth. The fault plane is consistent with the SW dipping plane of the Global Centroid Moment Tensor solution. The geodetic moment corresponding to our optimal solution is 2.38e+16 N·m, which is consistent with the GCMT seismic (2.19e+16 N·m). See Methods and supplementary material (figures S4, S5 and Table S1) for more details on the inversion procedure.

Golfo de San Jorge (GSJ) basin results

This section follows an analogue structure as the previous one. The available data for the study of the GSJ basin include displacement measurements obtained with InSAR methods, monthly volumes of conventional wells production and seismic data (a single event). In this basin, there is no relevant presence of non-conventional wells.

Figure 6 shows displacement velocity maps obtained using the Small Baseline approach (SBAS) (Casu et al. 2014) implemented at the Geohazards TEP platform. Fig 6a has been obtained from 85 Sentinel-1 SLC-IW images acquired in descending trajectory covering the period from 10th October 2017 to 24th September 2020. Fig 6b has been obtained from 48 Sentinel-1 SLC-IW images acquired in ascending trajectory between 1st of October 2017 and 12th of May 2019.

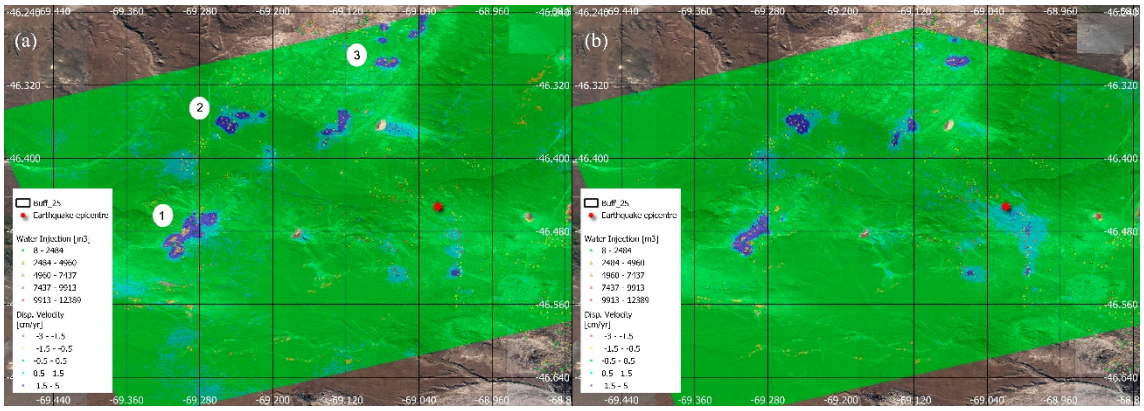

Figure 6: Line-Of-Sight (LOS) ground displacement velocity maps obtained with data acquired in ascending trajectory (a) and descending trajectory (b) in the GSJ basin. The time span is from 10th October 2017 to 24th September 2020 for the descending dataset and from 1st of October 2017 to 12th of May 2019 for the ascending one. Positive LOS values are movements towards the satellite. (1, 2, 3) point the areas with higher rates. The red star indicates the location of the M_L 5 2019 October 17 earthquake epicentre.

The colour scale represents the LOS displacement velocity of each point in cm/year. The estimated precision is ±1.3 mm/year and ±1.6 mm/year for the descending and ascending datasets, respectively. Time series precision is estimated as 3.7 mm for the ascending case and 3.9 mm for the descending.

For this study, areas of ground displacement identified in Figure 6 as zones 1 to 3 and the coseismic deformation marked with a star are analysed in detail.

Hydrocarbon production in GSJ basin and surface deformation

The displacement rates measured using the ascending trajectory show higher values than the descending one in the active zones detected (Figure 6). A clear example is observed in zone 1, where the north-east corner shows a clear blue sector in the ascending result which is less visible in the descending dataset. In this particular case, the difference can be explained by a horizontal component of the movement explained by the local topography of the area which is south-west oriented. The main differences in the rest of the sectors are explained because most of the movements occurred between 2017 and the first half of 2018. Thus, the results obtained using the ascending trajectory show higher displacement rates because the estimation period is shorter. However, the time series shown in Figure 7 (b, c and d) display similar magnitudes for the ascending and descending trajectories. Thus, according to these observations, we can conclude that the displacements are almost vertical and hence, uplifts.

The average displacement time series estimated for zones 1, 2 and 3 using the ascending and descending trajectories (red and yellow lines, respectively) are shown in Figure 7 (b, c and d). The red lines represent the standardised fluid balance production for recovery wells placed within these areas. Those are wells that, at some moment during the period analysed, showed water injection values over 0 m^3 and not only extraction values, allowing the calculation of the accumulated fluid balance (by fluid balance we refer to injected water minus extracted fluids, both for water and hydrocarbons). The standardisation process, which has been applied to make the production trends comparable to the ground deformation, is described in the Methods section.

Figure 7. (a) Production trends for the last 15 years in an area of 5 km radius that includes the 223 wells (with an average depth of 1.5 km) located around the 2019 October 17 earthquake epicentre (red dot in Figure 6) in the GSJ basin. Fluid (water and hydrocarbons) extraction (dark blue) and injection (water, lighter blue) and balance between them (injection minus extraction, green). The date of the occurrence of the earthquake is indicated by a vertical line in the chronological axis. The earthquake occurs immediately after the highest injection historic peak and in the strongest and sudden historical unbalance. (b, c, d) *Plots of time-series of deformation (red line for ascending orbit, yellow for descending orbit) and standardised fluid balance (green) for wells over the deformation zone labelled 1,2,3 in Figure 6 (a). (b) represents the trends of 54 recovery wells inside deformation zone 1, (c) 10 wells in zone 2, and (d) 3 wells in zone 3. Besides the standardisation, the scale bar in the right vertical axis provides the magnitude of the accumulated fluid balance during the analised period for the whole deformation zone.*

Hydrocarbon production in GSJ basin and the associated seismic events

Figure 7 (a) shows the harmonized data of the accumulated production and fluid balance of an area of 5 km around the epicenter of the 17th of October 2019.

No earthquakes were registered in the GSJ basin before October 2019. The only seismic event registered in the study area to date occurred on 17 October 2019 at 16:58:28.55 UTC, with a local magnitude of M_L5 according to INPRES moment magnitude (M_w) of 4.9 and 10 km depth according to the USGS (USGS, 2021). The location of the epicenter and depth of the earthquake varies among different agencies (USGS: latitude 46.401°S, longitude 69.070°W, 10 km depth; INPRES: latitude 46.284°S, longitude 68.734°W, 15 km depth; ISC: latitude 46.421°S, longitude 69.043°W, 10 km depths).

This seismic event induced ground deformation measurable with InSAR data. We have used the information provided by coseismic interferograms to constrain the earthquake source parameters. Figure 8 shows ground deformation associated with the earthquake in both ascending and descending geometry. This deformation pattern corresponds to a main lobe with a maximum ground displacement of ~ 35 mm towards the satellite and ~40 mm away from the satellite. This deformation pattern can be explained using a uniform slip rectangular dislocation (Fig. 8) centered at latitude -46.4529°S, longitude 69.0196°W (Fig. 5) and at 1.17 km depth. The inversion allows to locate the source of the event. The fault plane is consistent with the SW dipping plane of the Global Centroid Moment Tensor solution. The geodetic moment corresponding to our optimal solution (5.28e+16 N·m) is higher than the GCMT seismic moment (2.32e+16 N·m), which might

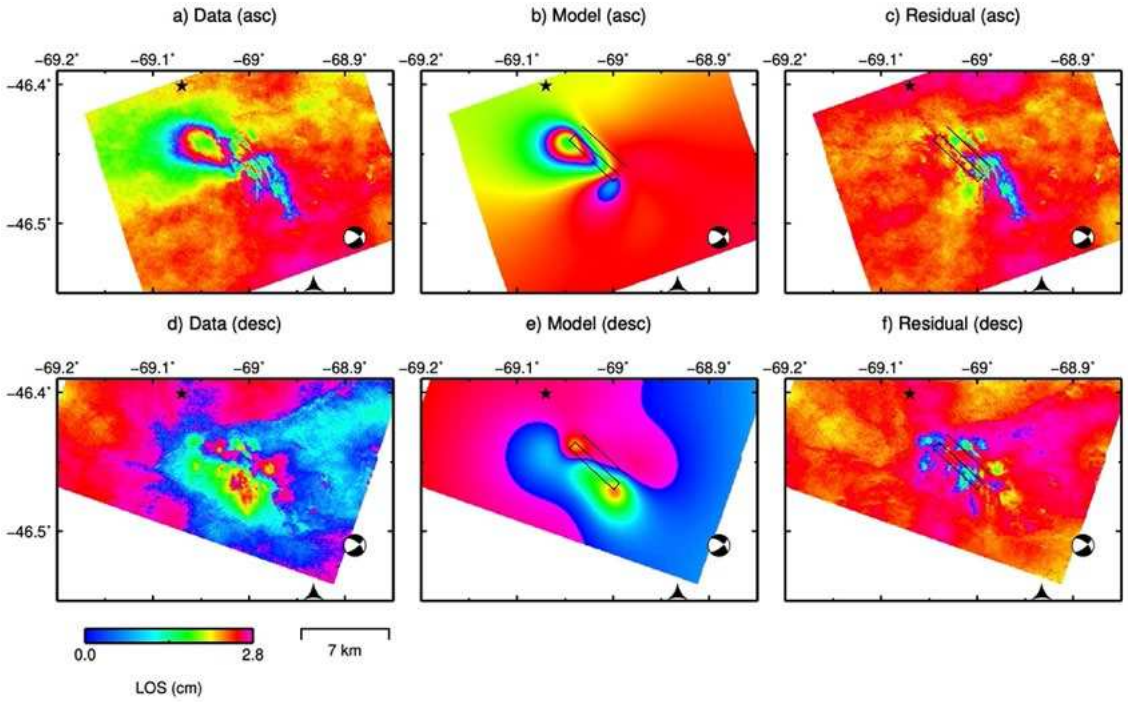

Figure 8. (a) and (d) show co-seismic Line-Of-Sight (LOS) deformation of the M_L 5, 2019 October 17 Las Heras earthquake obtained as the average of 4 and 6 co-seismic ascending and descending interferograms, respectively. (b) and (e) show LOS deformation predicted by the forward model using the maximum a posteriori probability solution. (c) and (f) show the residuals. The black rectangle represents the outline of the optimal fault plane, and the beach ball represents the fault plane solution from The Global Centroid Moment Tensor (GCMT).

be explained by the presence of post-seismic deformation in the co-seismic interferograms (since they span a post-seismic period of 43 days). See Methods and supplementary materials (figures S6, S7 and Table S2) for more details on the inversion procedure.

3 Discussion and conclusions

Two different types of phenomena occurring in two different regions of the Patagonian oilfields, the Neuquén basin and the Golfo de San Jorge basin, have been observed and analysed. For each site, we analysed the relation between surface ground displacements and earthquakes occurred around active well fields and hydrocarbon production operations.

In the Neuquén basin, the focus of the analysis is a zone of intense production of non-conventional hydrocarbons, in the region known as Vaca Muerta. We used DInSAR and PSI techniques to measure the ground displacements of the area. We detected ground displacement due to different sources. Two areas affected by subsidence were detected around two sets of wells. These areas are indicated as 1 and 2 in Figure 2. The analysis of these areas demonstrated a direct relationship between well production activities and ground surface displacement. First, we analysed two different temporal intervals, one before the start of operations (from October 2016 to March 2018) and a second one covering an active period (from October 2017 to 2020). The results obtained show that there was no ground movement during the absence of fracking wells, and that ground movement started a few months after the initiation of fracking operations. Moreover,

the collected data about the production activity show a clear unbalance between extraction and injection which fits very well with the type of detected movement (subsidence). The results analysis allows us to confirm the link between wells production and ground subsidence in the studied area.

We also analysed the seismic events occurred during the study period. On the one hand, our InSAR analysis revealed a second deformation phenomena related to the M_w 5 earthquake that occurred on 7th March 2019. The coseismic interferograms allowed us to precisely locate the source. On the other hand, our analysis of the seismic data and the production history allowed us to conclude that a correlation exist between the accumulated released seismic energy and the volume changes due to the injection and extraction activities:

- The production data show that in the observed area the hydrocarbon industry started with non-conventional wells in 2017 and that a few months later the seismic activity started.
- The data show that hydraulic fracturing rates and operated fluid volumes were exceptionally high (in local and global terms) immediately prior to the largest seismic events.
- Multiple wells were fracturing simultaneously in the same pad in a very reduced area.
- The largest seismic events occurred immediately after the highest hydraulic injection rates.
- The largest earthquake (M_w 5 2019 March 7) was very shallow according to our optimal source model (1.2 km depth).
- The comparison of the accumulated seismic energy with the subsurface volume changes due to the conventional and non-conventional production shows also a high level of correlation.

As shown in our analysis of seismicity in the Neuquén basin (Fig. 4), a sharp increase of the released seismic energy appears in relationship with the increase of extraction by fracking. However, the later attenuation of seismic energy suggests that the main component responsible for triggering induced earthquakes could be the injection.

A similar analysis has been performed in the GSJ area. Although the characteristics of the area are rather different, similar analysis allowed us to link ground displacements processes with hydrocarbon operations. As in the Neuquén basin test site, we have studied two types of ground displacements: uplift processes around exploitation wells during the monitored period and a single displacement event related to the M_w 4.9 earthquake occurred on 17th October 2019.

We focused the analysis of the uplift phenomena in 3 of the most significant areas, labelled 1, 2 and 3 in Figure 6. The comparison between uplift phenomena and hydrocarbon exploitation shows that there is a very good agreement between the fluid balance that is almost positive and the uplift during the measured period, suggesting a cause-effect relationship.

The seismicity in the GSJ study area shows a different behaviour than the Neuquén example. In this case, there is a single event, with no seismicity recorded in the area before or after this event. Furthermore, in this case the main activity in the area around the earthquake epicentre during the monitored period was fluid injection. The highest injection historic peak and the strongest historic unbalance between fluid injection and

extraction in this location occurred just some days before the earthquake, see Figure 7 (a). The coseismic interferograms allowed us to locate the earthquake at a very shallow depth (1.17 km), which is consistent with the well depth. These three facts, shallow earthquake source, absence of record of prior and post seismic events, and the extraordinary peak of injection suggest that this event was directly related with the wells operations.

Both cases are two very interesting and different examples where the correlation between seismicity and hydrocarbon operation can be clearly shown. They represent very good examples of how this industry can affect the environment by changing the geological equilibrium, producing ground displacement and triggering earthquakes in areas without existing prior seismicity. Moreover, the cases studied in this work affected the population living around the exploitation areas, producing social unrest that in some cases culminated in the halting of operations. One question that raises up thorough these cases is if those events could be avoided with better characterization of the exploitation sites and with better planning of the injection-extraction activities. These are open questions nowadays but must be addressed by both industry and public administration. This is, for example, especially critical nowadays in Europe where some potential non-conventional exploitation of huge gas reservoirs have been stopped due to the strong opposition of the local population.

Another important point to be considered are the ground displacements that such activities produce and that can potentially produce damages for different reasons, such as infrastructures affectation (pipes, towers and others) and thus the safety during the operations, or groundwater contamination affecting the local population. Thus, the characterization of both, subsurface and surface phenomena, is necessary to prevent potential problems.

These examples are in line with previous works available in the literature and confirm the need for improvement of the hydrocarbon industry and the whole society to properly prevent induced geohazards and their consequences. In our study case, fluid leaks, explosions and fires linked to the operations, atmosphere and water pollution, damage of diverse infrastructures, and other potential damages are not being correctly assessed due to the absence of prevention policies. For example, both sites of this study are considered non seismic by the INPRES national seismic hazard zonification (INPRES 2021b) due to the absence of seismic events in historical terms. This means that the construction normative does not consider anti-seismic criteria in the area (even for the structures related to the new wells). In the GSJ basin the situation seems less alarming as only one event has been registered. However, the almost absolute absence of a scientific and public debate about the link between the industry and the earthquakes and its consequences, risks reproducing and aggravating the experiences lived in the last few years.

Methods

This section describes the dataset and methods used in this work.

SAR datasets

In this work have been used 5 different independent Sentinel-1 IW SAR datasets. One for each trajectory of the satellite (ascending and descending) for each test site. The

Neuquén basin descending dataset is divided in two: 32 images covering a period previous to operations in the area, October 2016 to March 2018 and 41 images covering a period that includes wells operation and the main earthquake event, October 2018 to April 2020. The ascending dataset consisted of 56 images covering the period February 2018 to April 2020.

The GSJ basin dataset consisted in 85 descending images acquired between October 2017 and September 2020 and 48 ascending images covering the period October 2017 to May 2019. The main earthquake event in the area is within the covered periods. The tables showing the full list of images are in the supplementary material.

InSAR processing

Two different processors have been used to obtain the PSI results: the PSIG chain developed by the CTTC and described in Devanthery et al. (2014) and the Parallel Small Baseline Subset (P-SBAS) approach (Casu et al. 2014, Manunta et al. 2019) available on the Geohazards TEP platform.

The PSIG approach has been used to process the operations period of the Neuquén site: 2018-2020. The main results provided by the approach are the displacement velocity maps and the temporal behavior of each measured PS. The temporal coherence threshold to select PSs is set to 0.7. The images are processed at full resolution. The main figures of the results are discussed in section 2.

The GSJ datasets and the 2016-2018 dataset over the Neuquén site have been processed using the P-SBAS approach implemented at the Geohazards TEP platform. The main results provided by the approach are mean LOS displacement velocity maps and LOS displacement time series of each measured pixel. The temporal coherence threshold to select a coherent pixel is set to 0.85. The spatial resolution is ~70 m (multilook applied: 20 in range x 5 in azimuth).

Finally, the coseismic interferograms have been processed by the CTTC interferometric processor. The interferograms have been unwrapped using the unwrapping approach described in Constantini, 1998. We calculated an average interferogram for each earthquake, in ascending and descending geometry, averaging 11 coseismic ascending interferograms and 10 coseismic descending interferograms for the M_L 4.9, 2019 March 7 Neuquén basin earthquake and 4 coseismic ascending interferograms and 6 coseismic descending interferograms for the M_L 5, 2019 October 17 GSJ basin earthquake. See the supplementary material for details.

Hydrocarbon production and injection volumes

The wells' location and production data were downloaded from official public databases from the Argentine Energy Secretariat. The database provides an accurate description of the wells and information about owner company, well depth, well status (abandoned, operative), etc. Monthly production disaggregated information is reported for each well and fluid type (natural gas, oil, water). The same happens for the hydraulic fracturing process: injected materials, operating pressure and period, fracture stages quantity, horizontal branch length and some other information is provided.

All production quantities are given in cubic metres (m^3), except injected sands and produced gas. Sands are given in metric tonnes that have been converted to m^3 to allow comparisons. Gas is informed in thousands of m^3 in standard conditions (1 bar and 288

K). We have converted them to equivalent m^3 at reservoir conditions, applying PVT essential relations and the corresponding compressibility factor. This transformation allowed us to approximate the actual displaced volume from the geological formation. Oil and water volumes need no conversion. In the Neuquén basin, the studied wells are almost exclusively gas producers and gas is extracted around 3000 m beneath the surface, so determining the correct gas conversion factor is essential to understand the processes. Assuming typical pressure and temperature values for the formation we equated 1000 m^3 of gas in standard conditions to 2 m^3 beneath the surface. In the GSJ basin case (black oil), gas production has a negligible contribution, so a coarse approximation is valid for the analysis. Considering the scarce information about the physical conditions in the GSJ formations, we applied the same gas volume factor as in the Neuquén basin. In the GSJ basin, the variable truly controlling the production trends is water injection and extraction, and secondly, oil production, which in the area is around 10 times smaller than the water one.

We have scaled the production data to ease the comparison between ground deformation [mm] and production processes [m^3]. Depending on a) the type of activity (injection or extraction, conventional or not), b) the number of involved wells in the displacement phenomena and c) the extension of the affected area, the amounts of fluid causing ground deformation can be considerably diverse. So, referring to the total nominal amount may mislead when observing different cases. For example, in Figure 7 a balance volume in panel (b) which is more than two times bigger than in panel (d) produces equivalent deformation. This is explained because of the size of each affected area and the number of wells covering it (the density of wells by area unit and the total area size). Consequently, we standardised the production data. First, monthly amounts have been represented as a fraction of the total accumulated for the study period, as a per one ratio. Then, the curve has been scaled to fit the same numeric scale as ground deformation (we multiplied the monthly normalised production rate by the average of the accumulated ascending and descending deformation of each case and period). In the case of the subsidence, zones 1 and 2 of the Neuquén basin where the process is linked to the gas extraction, the curve has been inverted. All the data processed is available in the supplementary material.

Seismic data

Both regions are deficiently covered by a seismic network, only few seismographs are sited hundreds of kilometres away of the study areas. This could explain the low b-value obtained from the seismic dataset (see supplementary data). One can consider a catalogue magnitude of completeness > 2.4 M_L for at least the last decade facilitated by the INPRES, with an associated error of around 20 km in epicentre and hypocenter determination. In the Neuquén basin, before 2018, only a M_L 4.5 event in 2015 and a M_L 4.3 event in 2017 were reported, and more than two hundred since 2018. In the GSJ basin, apart from the M_L 5 2019 October 17th earthquake studied here, no seismic events were reported. The statements above are independent of the magnitude or historic period in both study areas (INPRES, 2021). To better adjust to scientific standards, the data corresponding to the most important events (M_L > 4) have been taken from the USGS database. Nevertheless, the seismic catalogue can be considered complete for earthquakes magnitudes M_L > 4.5 from the second half of the twentieth century attending to international agencies as USGS and ISC and historic reports.

Modelling coseismic deformation

The source modelling was performed using the freely available Geodetic Bayesian Inversion Software (GBIS) (Bagnardi and Hooper 2018), which allows the estimation of the optimal source model parameters using a Bayesian approach for the inversion of multiple geodetic data sets. The inversion was carried out using a rectangular dislocation source within an elastic half-space (Okada, 1985), with nine source model parameters (length, width, depth of the upper edge, dip angle, strike, X and Y coordinates of the midpoint of the upper edge, slip in the strike direction and uniform slip in the dip direction).

The GBIS software characterised the errors in each independent InSAR data set, such as randomly distributed noise and spatially correlated phase delays, by estimating variance and covariance in non-deforming areas. A linear ramp was also estimated during the inversion to remove any residual orbital error or very long wavelength atmospheric delay across the entire InSAR data sets.

The InSAR data subsampling carried out in GBIS, which uses a quadtree algorithm, resulted in 142 points for the Neuquén basin ascending data (from 83.611 initial points); 136 points for the Neuquén basin descending data (from 83.302 initial points), 176 points for the GSJ basin ascending data (from 128.546 initial points) and 214 points for the GSJ basin descending data (from 164.113 initial points). See Supplementary Figs. S4 and S6.

The results for the optimal nine fault source parameters and associated uncertainties in each case were obtained after 10^6 iterations. The optimal parameters are extracted from the posterior probability density functions by finding the maximum a posteriori probability solution.

Data availability

- Public Argentinian hydrocarbon production reports and wells specifications are freely on-line available at the official webpage: https://datos.gob.ar/dataset/energia-produccion-petroleo-gas-por-pozo-capitulo-iv
- Sentinel 1 ESA SAR Satellite images are freely on-line available at the offical site: https://scihub.copernicus.eu/dhus/
- Processed datasets derived from these raw data are open. Authors can share under request.

References (limited to 60 references, though not strictly enforced)

Atkinson, Gail & Assatourians, Karen & Cheadle, Burns & Greig, Wes. (2015). Ground Motions from Three Recent Earthquakes in Western Alberta and Northeastern British Columbia and Their Implications for Induced-Seismicity Hazard in Eastern Regions. Seismological Research Letters. 86. 1022-1031. 10.1785/0220140195.

Bagnardi, M., and Hooper, A. (2018). Inversion of surface deformation data for rapid estimates of source parameters and uncertainties: A Bayesian approach. Geochemistry, Geophysics, Geosystems, 19(7), 2194-2211.

Baranova, Valentina & Mustaqeem, Azer & Bell, Sebastian. (2011). A model for induced seismicity caused by hydrocarbon production in the Western Canada Sedimentary Basin. Canadian Journal of Earth Sciences. 36. 47-64. 10.1139/cjes-36-1-47.

Chen, Xiaowei & Nakata, Nori & Pennington, Colin & Haffener, Jackson & Chang, Jefferson & He, Xiaohui & Zhan, Zhongwen & Ni, Sidao & Walter, Jacob. (2017). The Pawnee earthquake as a result of the interplay among injection, faults and foreshocks. Scientific Reports. 7. 10.1038/s41598-017-04992-z.

Correa-Otto, S. (2021) Experimento sismológico en la Cuenca Neuquina, la región de mayor explotación de hidrocarburos por métodos no convencionales de la Argentina. Universidad Nacional de San Juan. FCEFyN. Instituto Geofísico Sismológico Volponi.

Devanthéry, Núria & Crosetto, M. & Monserrat, O. & Cuevas-González, María & Crippa, B.. (2014). The PSIG chain: An approach to Persistent Scatterer Interferometry. Remote Sensing. 6. 6662-6679. 10.3390/rs6076662.

Ellsworth, W. L. Injection-Induced Earthquakes . Science 341, 1225942 (2013). DOI: 10.1126/science.1225942

Grigoli, Francesco & Cesca, Simone & Rinaldi, Antonio Pio & Manconi, Andrea & López-Comino, José-Ángel & Clinton, John & Westaway, Robert & Cauzzi, Carlo & Dahm, Torsten & Wiemer, Stefan. (2018). The November 2017 Mw 5.5 Pohang earthquake: A possible case of induced seismicity in South Korea. Science. 360. 10.1126/science.aat2010.

INPRES (2021a) INRPES. Buscador de sismos. http://contenidos.inpres.gob.ar/buscar_sismo

INPRES (2021) INRPES. Zonificiación sísmica. http://contenidos.inpres.gob.ar/acelerografos/Reglamentos#Zonificaci%C3%B3n%20S%C3%ADsmica

ISC (2021) International Seismological Centre. http://www.isc.ac.uk/iscbulletin/search/catalogue/

Kim, Jin-Woo & Lu, Zhong. (2018). Association between localized geohazards in West Texas and human activities, recognized by Sentinel-1A/B satellite radar imagery. Scientific Reports. 8. 10.1038/s41598-018-23143-6.

Kim, Kwang-Hee & Ree, Jin-Han & Kim, YoungHee & Kim, Sungshil & Kang, Su & Seo, Wooseok. (2018). Assessing whether the 2017 M w 5.4 Pohang earthquake in South Korea was an induced event. Science. 360. eaat6081. 10.1126/science.aat6081.

Lei, Xinglin & Huang, Dongjian & Su, Jinrong & Jiang, Guomao & Wang, Xiaolong & Wang, Hui & Guo, Xin & Fu, Hong. (2017). Fault reactivation and earthquakes with magnitudes of up to Mw4.7 induced by shale-gas hydraulic fracturing in Sichuan Basin, China. Scientific Reports. 7. 10.1038/s41598-017-08557-y.

Okada, Y. (1985). Surface deformation due to shear and tensile faults in a half-space. Bulletin of the seismological society of America, 75(4), 1135-1154.

Samsonov, Sergey & Feng, Wanpeng & Fialko, Yuri. (2017). Subsidence at Cerro Prieto Geothermal Field and postseismic slip along the Indiviso fault from 2011 to 2016 RADARSAT-2 DInSAR time series analysis. Geophysical Research Letters. 10.1002/2017GL072690.

Shirzaei, M., Ellsworth, W. L., Tiampo, K. F., González, P. J., & Manga, M. (2016). Surface uplift and time-dependent seismic hazard due to fluid injection in eastern Texas. Science, 353(6306), 1416-1419.

USGS (2021) Latest earthquakes. USGS. https://earthquake.usgs.gov/earthquakes/map/

YPF. 2021. https://www.ypf.com/desafiovacamuerta/Paginas/vaca-muerta.html

Vásquez, J. Spagnotto, S. Mescua, J.F., Giambiagi, L. y Sigismondi, M. (2020). Aumento notorio de la sismicidad de la provincia del Neuquén, en el período 2015-2020. Boletín Brackebuschiano, Asociación Geológica Argentina. ISSN: 0328-2724

Vázquez, Joaquín & Spagnotto, Silvana & Giambiagi, Laura & Sigismondi, Mario & Mescua, José. (2021). Aumento notorio de la sismicidad - provincia del Neuquén, período 2015-2020. 2. 1 - 13.

Weingarten, Matthew & Ge, Shemin & Godt, Jonathan & Bekins, Barbara & Rubinstein, Justin. (2015). INDUCED SEISMICITY. High-rate injection is associated with the increase in U.S. mid-continent seismicity. Science (New York, N.Y.). 348. 1336-40. 10.1126/science.aab1345.

Acknowledgements

Thanks to Red Geocientífica Chile and Observatorio Petrolero Sur for sharing their information about the industry geohazards. Project supported by ESA Network of Resources Initiative and project PID2020-116540RB-C22 funded by MCIN/AEI /10.13039/501100011033 and Grant FPU19/03929 funded by MCIN/AEI/10.13039/501100011033 and by "FSE invests in your future". This work was partially developed under the objective of the project FAMRAD, nº of agreement PID2020-113407RB-I00. Figures were prepared using the public domain GMT, QGIS, LibreOffice and Inkscape software's. The authors would like to thank the people living and working in Sauzal Bonito who helped us to understand the causes and consequences of the seismicity in the area.

Author contributions

G. T. B., M.B.P. and O.M. coordinated the team. G.T.B processed the hydrocarbon production data. M.B.P. performed the SBAS and the seismic modelling analysis, the last, together with J.J.P.F. O.M. performed the PSI analysis. R.P.L. calculated the seismic energy release. M.C. made the materials volumetric conversions. J.G. supervised the agreement between the data reports and the on the field industrial activity.

Additional Information (including a Competing Interests Statement)

The authors declare no competing interests.

Figure legends (these are limited to 350 words per figure)

Figure 1. Study areas in the Argentinian Patagonia. Data are plotted on SRTM topography (Farr and Kobrick 2000) displayed in shaded relief. (A) Neuquén basin area. Blue circles represent epicenters of seismic events scaled by local magnitude (M_L) occurred in the period November 2015 to November 2020, from the Instituto Nacional de Prevención Sísmica (INPRES) catalog. The red cross indicates the reference point for the 15-km screening criterion analyzed in figure 3. The location of fracking (black triangles) and wastewater (green triangles) wells is also shown (Secretaría de Energía). Black lines indicate the main tectonic faults from Silvestro and Zubiri (2008). The Global Centroid Moment

Tensor (GCMT) focal mechanism of the 07/03/2019 earthquake (M_L 4.9, M_w 5) is shown. (B) Golfo de San Jorge area. Brown triangles represent production wells. Black lines indicate the main tectonic faults (Allard et al, 2020). The red cross indicates the reference point for the 5-km distance limit analyzed in figure 3. The Global Centroid Moment Tensor (GCMT) focal mechanism of the 17/10/2019 earthquake (M_L 5, M_w 4.9) is shown. (C) Inset map showing the region of South America with the two study areas delineated in blue (Neuquén basin) and red (GSJ basin).

Figure 2. Average Line-Of-Sight (LOS) ground displacement velocity maps obtained exploiting the PSI techniques observed with a descending trajectory spanning the period from February 2018 to April 2020 (a) and with an ascending trajectory from October 2018 to April 2020 (b). Positive and negative LOS values represent ground displacements towards and away from the satellite, respectively. Main deformation zones labelled 1 and 2 correspond to areas with high concentration of wells, 33 and 25 respectively (see Figure 1). Label 3 indicates the main area affected by the M_L 4.9, 2019 March 7 earthquake.

Figure 3. (a) Temporal evolution of hydrocarbon production (in m3) during the period 2015 – 2020 in the Neuquén basin. Main seismic events in the area are shown as vertical dashed black lines. Panels (b) and (c) show the time series of ground deformation for zones 1 and 2, respectively, during the period 2018-2020 together with monthly accumulated non-conventional gas production. This last curve has been normalised, from 0 to 1 for the time span, and inversely scaled to fit the same nominal scale as deformation patterns. The vertical scale bar in the right axis of figures (b) and (c) provide information on the total accumulated volumetric amount (m3) of non-conventional gas extracted.

Figure 4. Accumulated seismic energy released (in Joules) recorded by INPRES between 2015 and 2020, versus different underground operations within the Neuquén basin study area (in m^3). Blue and green lines show injected and extracted fluid volume, respectively, using non-conventional methods. Purple line shows extracted fluid volume using conventional methods. The production data used for this figure are the same used in Figure 3.

Figure 5. (a) and (d) show coseismic Line-Of-Sight (LOS) deformation of the Mw 5, 2019 March 7 Neuquén basin earthquake obtained as the average of 11 coseismic ascending interferograms (in a) and as the average of 10 coseismic descending interferograms (in d). (b) and (e) show LOS deformation predicted by the forward model using the maximum a posteriori probability solution. (c) and (f) show the residuals. The black rectangle represents the outline of the optimal fault plane. The Global Centroid Moment Tensor (GCMT) is represented by the beach ball.

Figure 6: Line-Of-Sight (LOS) ground displacement velocity maps obtained with data acquired in ascending trajectory (a) and descending trajectory (b) in the GSJ basin. The time span is from 10th October 2017 to 24th September 2020 for the descending dataset and from 1st of October 2017 to 12th of May 2019 for the ascending one. Positive LOS values are movements towards the satellite. (1, 2, 3) point the areas with higher rates. The red star indicates the location of the M_L 5 2019 October 17 earthquake epicentre.

Figure 7. (a) Production trends for the last 15 years in an area of 5 km radius that includes the 223 wells (with an average depth of 1.5 km) located around the 2019 October 17 earthquake epicentre (red dot in Figure 6) in the GSJ basin. Fluid (water and hydrocarbons) extraction (dark blue) and injection (water, lighter blue) and balance between them (injection minus extraction, green). The date of the occurrence of the earthquake is indicated by a vertical line in the chronological axis. The earthquake occurs immediately after the highest injection historic peak and in the strongest and sudden historical unbalance. (b, c, d) *Plots of time-series of deformation (red line for ascending orbit, yellow for descending orbit) and standardised fluid balance (green) for recovery wells over the deformation zone labelled 1,2,3 in Figure 6 (a). (b) represents the trends of 54 recovery wells inside deformation zone 1, (c) 10 wells in zone 2, and (d) 3 wells in zone 3. Besides the standardisation, the scale bar in the right vertical axis provides the magnitude of the accumulated fluid balance during the analised period for the whole deformation zone.*

Figure 8. (a) and (d) show co-seismic Line-Of-Sight (LOS) deformation of the M_L 5, 2019 October 17 Las Heras earthquake obtained as the average of 4 and 6 co-seismic ascending and descending interferograms, respectively. (b) and (e) show LOS deformation predicted by the forward model using the maximum a posteriori probability solution. (c) and (f) show the residuals. The black rectangle represents the outline of the optimal fault plane, and the beach ball represents the fault plane solution from The Global Centroid Moment Tensor (GCMT).

Tables

Supplementary Files

This is a list of supplementary files associated with this preprint. Click to download.

- SupplementaryDataset.zip